Electronic Supplementary Information

Engineering Mn–Co–Cu hydroxide/oxyhydroxide electrode materials: rational composition optimization for enhanced supercapacitor performance

Venkatesan Gowsalya,[a] Sankar Sarathkumar,[a] Raji Yuvaraja,[a] Sorna Pandian Anitha Juliet,[a] Selvakumar Veeralakshmi,[b] and Selvan Nehru*[a]

[a]Department of Physical Chemistry, University of Madras, Guindy Campus, Chennai - 600025, Tamilnadu, India.
[b]Centre for Industrial Safety, Anna University, Chennai - 600025, Tamil Nadu, India.

1. Materials and methods

All chemicals used in this study were of analytical grade and used as received without further purification. Copper(II) chloride dihydrate, cobalt(II) chloride hexahydrate, manganese(II) chloride tetrahydrate, sodium carbonate, sodium hydroxide, potassium hydroxide, and N-methyl pyrrolidine (NMP) were purchased from Sisco Research Laboratories Pvt. Ltd. Acetylene black carbon (C_{AB}) and polyvinylidene fluoride (PVDF) were purchased from Sigma-Aldrich. Polyvinyl alcohol (PVA, Mw = ~115,000) was obtained from Loba Chemie Pvt. Ltd. Deionized (DI) water was utilized throughout the experiments. Before use, nickel plate (99% purity, thickness: 0.5 mm) was polished with P220 emery paper to activate the surface, then sequentially cleaned in 1 M HCl for 15 minutes and followed by in acetone for 30 minutes using ultrasonication to remove any surface residues.

2. Materials characterization

X-ray diffraction (XRD) patterns of samples were obtained using a PANalytical X-ray diffractometer with Cu-Kα radiation as the X-ray source in the 2θ range of 10°–80°. Fourier transform infrared (FT-IR) spectroscopy was carried out on a SHIMADZU spectrometer. The thermogravimetric analysis (TGA) of the samples was performed using a TGA Q500 V20.13 Build 39 thermal analyzer in a nitrogen atmosphere from ambient temperature to 750 °C with a heating rate of 10 °C min^{-1}. X-ray photoelectron spectroscopy (XPS) was carried out on a PHI Versa Probe III Scanning XPS Microprobe, Physical Electronics, USA. Surface morphology and chemical elements of the samples were examined by a Nova NanoSEM (450) field emission scanning electron microscopy (FESEM) coupled with energy dispersive X-ray spectroscopy (EDS). High-resolution

transmission electron microscopy (HRTEM) was performed on a JEOL JEM-2100 Plus microscope. BET surface area and BJH pore size distribution of the samples were obtained from the N_2 adsorption–desorption isotherm technique using a Quantachrome Autosorb iQ instrument. All electrochemical measurements were carried out using the K-Lyte 1.3 (PG-Lyte) electrochemical workstation (Kanopy Techno Solutions, India). Electrochemical impedance spectroscopy (EIS) measurements were performed using the CHI660E workstation in the frequency range of 0.1 Hz to 100 kHz with a potential amplitude of 10 mV.

3. Three-electrode supercapacitor studies

To perform three-electrode SC studies, a platinum wire, a Hg/HgO electrode, and aqueous 3 M KOH were used as the counter electrode, reference electrode, and electrolyte, respectively. Further, the working electrode was made from the slurry consisting of active material (80 wt%), C_{AB} (10 wt%) as conducting material, and PVDF (10 wt%) as binder, using the requisite amount of NMP as solvent. Then the resultant slurry was coated on the surface of the nickel plate current collector (1.5 cm x 1.5 cm), followed by drying at 60 ^{o}C for 5 h. The mass loading of active materials on the nickel plate was calculated by weighing the plate before and after the loading of the active material. Cyclic voltammetry (CV) experiments were performed in the potential range of 0 to 0.6 V at various scan rates (10, 20, 40, 60, 80, and 100 mV s^{-1}) to capture the complete anodic and cathodic redox features. Galvanostatic charge-discharge (GCD) studies were assessed between the potential window of 0 to 0.5 V at different current densities (1, 2, 3, 4, 5, 10, and 15 A g^{-1}). Based on a comparative assessment of IR drop, coulombic efficiency, and discharge time, 0.50 V was chosen to ensure stable and reliable cycling behavior for GCD measurements. From the obtained GCD curves, three-electrode supercapacitor performance of the as-prepared electrode materials was assessed by using equations (S1 – S5).[1]

$$C_s\,(F/g) = \frac{I \times \Delta t}{m \times \Delta V} \quad \text{(S1)}$$

$$Q_s\,(mAh/g) = \frac{I \times \Delta t}{m \times 3.6} \quad \text{(S2)}$$

$$Q_s\,(C/g) = \frac{I \times \Delta t}{m} \quad \text{(S3)}$$

$$C_{areal}\,(C/cm2) = \frac{I \times \Delta t}{a \times \Delta V} \quad \text{(S4)}$$

$$\eta\ (\%) = \frac{t_d}{t_c} \times 100 \quad \text{(S5)}$$

where C_s (F g^{-1}) is specific capacitance, Q_s (mAh g^{-1}) is specific capacity, C_{areal} (F cm^{-2}) is areal capacitance, Q_s (C g^{-1}) is specific capacity, I (A) is constant discharge current, Δt (s) is time taken for discharging, ΔV (V) is potential drop upon discharging after excluding the instantaneous IR drop, m (g) is mass loading of the active material on the electrode, and a is electrode area (2.25 cm^2), t_d is the discharge time (s) and t_c is the charging time (s).

4. Two-electrode symmetric and asymmetric SC studies

For the two-electrode SC studies, symmetric SC was fabricated using a Swagelok-type cell by sandwiching the two symmetric electrodes using the Whatman filter paper as a separator and 3 M KOH as an electrolyte. The electrodes were made by coating the slurry of active material consisting of MnCoCu–1:5:1 (80 wt%), PVDF (10 wt%), C_{AB} (10 wt%) using NMP solvent on the two nickel plates (diameter: 1.7 cm and active area: 2.27 cm^2), followed by drying at 60 oC for 5 h. By following the same method, the asymmetric two-electrode SC was constructed, except that one of the electrodes consists of active material as C_{AB} (90 wt%) and PVDF (10 wt%). From the obtained GCD curves, the performance of the two-electrode SCs was assessed by using equations (S6–S12) for both symmetric and asymmetric configurations.

$$C_{s,\,cell} = \frac{I \times \Delta t}{m' \times \Delta V} \quad \text{(S6)}$$

$$Q_s\,(mAh/g) = \frac{I \times \Delta t}{m' \times 3.6} \quad \text{(S7)}$$

$$Q_s\,(C/g) = \frac{I \times \Delta t}{m'} \quad \text{(S8)}$$

$$C_{areal,\,cell} = \frac{I \times \Delta t}{a \times \Delta V} \quad \text{(S9)}$$

$$E = \frac{Cs,\ cell \times (\Delta V)2}{2 \times 3.6} \quad \text{(S10)}$$

$$P = \frac{E}{\Delta t} \times 3600 \quad \text{(S11)}$$

$$\eta\ (\%) = \frac{t_d}{t_c} \times 100 \quad \text{(S12)}$$

where E is the energy density (W h kg^{-1}), P is the power density (W kg^{-1}), and m' (= $m^+ + m^-$) is the total mass loading of the active materials in both anode and cathode (g).

For the asymmetric supercapacitor, the charge balance between the positive (cathode) and negative (anode) electrodes was determined using the equation (S13) to satisfy $q^+ = q^-$ (where q is the charge stored by each electrode).[5, 6]

$$m^+C^+\Delta V^+ = m^-C^-\Delta V^- \quad \text{(S13)}$$

where m is the active mass, C is the specific capacitance measured in three-electrode mode, and ΔV is the operating potential window of each electrode.

Based on this calculation, the optimized mass loading ratio (m^+/m^-) was fixed at 0.0286. The actual active masses used in the assembled device were 0.2531 mg cm^{-2} for the positive electrode and 8.8580 mg cm^{-2} for the negative electrode. The assembled asymmetric supercapacitor was operated within a stable cell voltage window of 0–1.4 V, which was selected based on cyclic voltammetry and galvanostatic charge–discharge tests with no observable polarization or electrolyte decomposition.

5. Fabrication of all-solid-state asymmetric SC

All-solid-state SC was fabricated using PVA-KOH gel electrolyte as follows: To a 30 mL aqueous warm solution of PVA (4 g), an aqueous solution of KOH (6 g, 20 mL) was added vigorously and maintained at 85 °C for 4 h until a clear solution was obtained.[2] For the positive electrodes, a slurry was prepared by mechanical grinding of materials, such as MnCoCu–1:5:1 (80 wt%) as active material, PVDF (10 wt%) as binder, and C_{AB} (10 wt%) as conductive agent using NMP solvent. This slurry was coated by doctor-blading onto three nickel plate current collectors (4.0 cm x 1.0 cm) and dried at 60 °C for 5 h. The same procedure was followed for negative electrode preparation, by taking C_{AB} as active material (90 wt%), and PVDF (10 wt%) as binder, using NMP solvent, and the slurry was coated by doctor-blading onto three nickel plate current collectors (4.0 cm x 1.0 cm) and dried at 60 °C for 5 h. After that, the as-prepared electrodes were dipped for 5 minutes in the hot PVA-KOH gel solution, then removed and allowed to solidify at room temperature. The as-coated PVA–KOH gel serves as both the electrolyte and the separator for the electrodes. Furthermore, a set of three sandwich-like asymmetric supercapacitor devices was fabricated and evaluated through open- circuit potential (OCP) measurements. Then, three sets of asymmetric supercapacitor devices were coupled in series and activated through the cyclic voltammetry method for 10 cycles. After charging, the device was tested to light a green LED to evaluate the supercapacitor performance for real-time applications.

6. t-plot (Halsey film-thickness model)

To quantitatively distinguish the contributions of micropores and mesopores, a Halsey t-plot analysis was carried out using the N_2 adsorption isotherm at 77 K in conjunction with the BET surface area results. The statistical thickness (t, in nm) of the adsorbed N_2 film was calculated using the standard Halsey equation (S14):[3, 4]

The film thickness (t, in nm), $$t = 0.354\left(-\frac{5}{\ln(P/P0)}\right)^{1/3} \quad \text{(S14)}$$

where, t is the thickness of the adsorbed N_2 film (nm), P/P_0 is the relative pressure, and the constants 5 and 1/3 are the standard Halsey parameters applicable for nitrogen adsorption at 77 K.

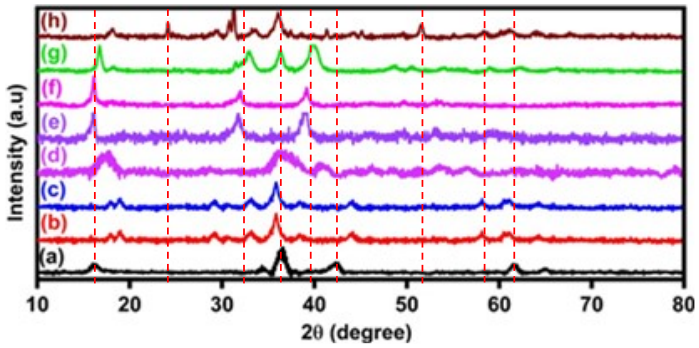

Fig. S1 Comparative XRD patterns of (a) MnCoCu–1:1:1, (b) MnCoCu–3:1:1, (c) MnCoCu– 5:1:1, (d) MnCoCu–1:3:1, (e) MnCoCu–1:7:1, (f) MnCoCu–1:9:1, (g) MnCoCu–1:1:3, and (h) MnCoCu–1:1:5.

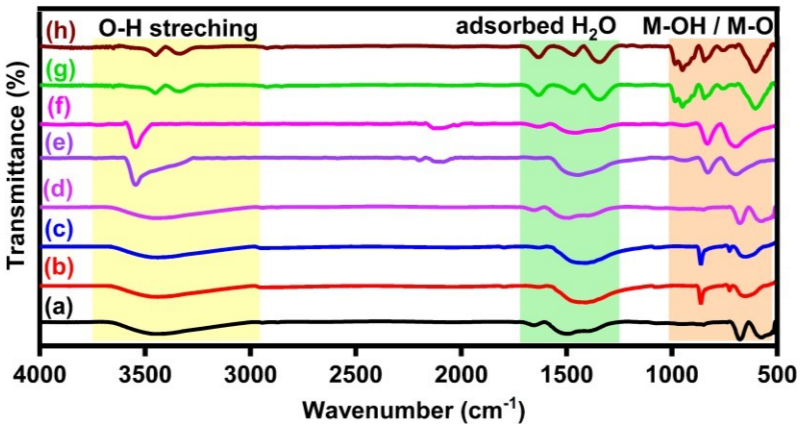

Fig. S2 Comparative FTIR spectra of (a) MnCoCu–1:1:1, (b) MnCoCu–3:1:1, (c) MnCoCu–5:1:1, (d) MnCoCu–1:3:1, (e) MnCoCu–1:7:1, (f) MnCoCu–1:9:1, (g) MnCoCu–1:1:3, and (h) MnCoCu–1:1:5.

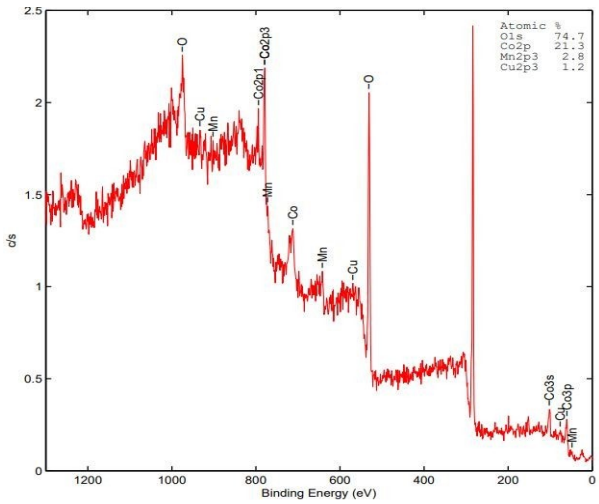

Fig. S3 XPS survey spectrum of MnCoCu–1:5:1.

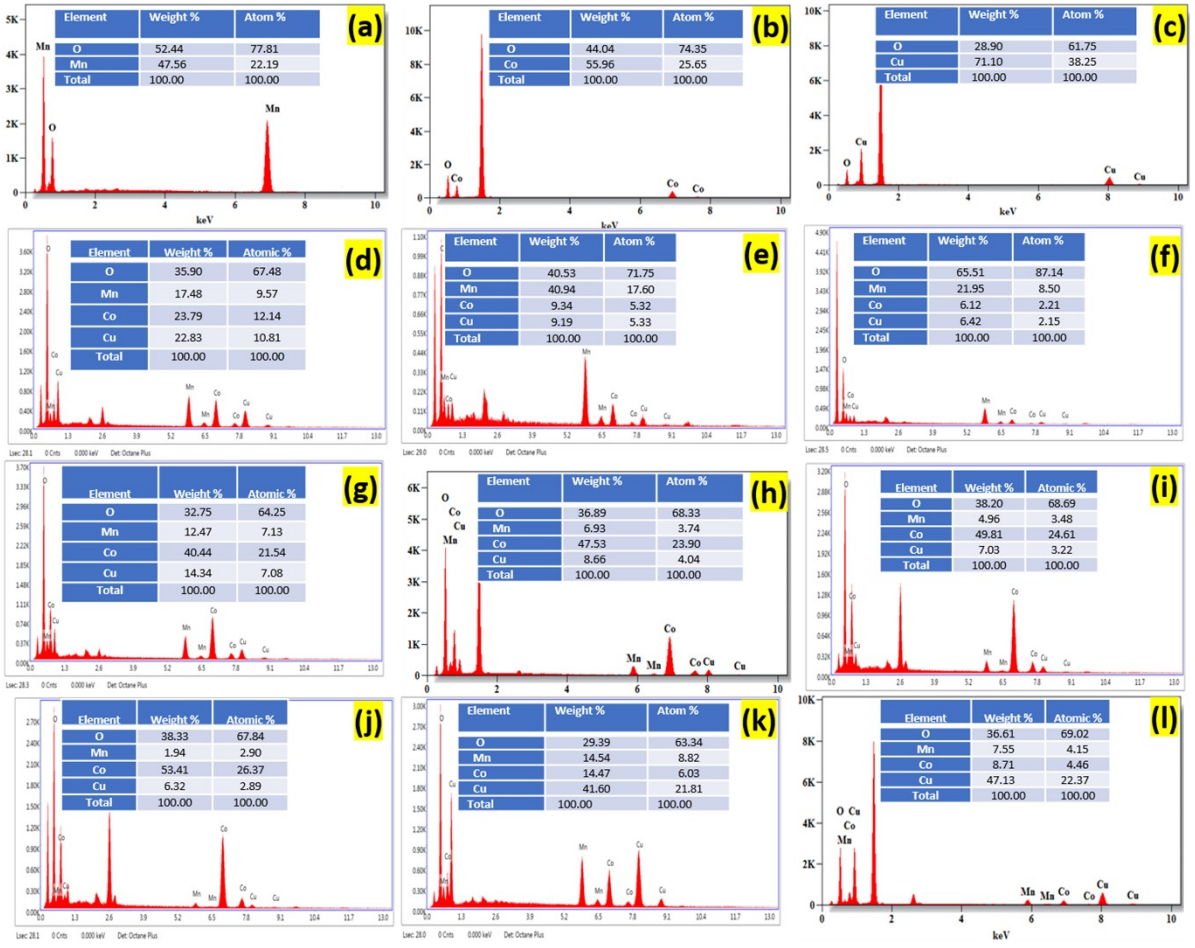

Fig. S4 EDAX spectra of as-prepared nanomaterials: (a) MnO(OH), (b) CoO(OH), (c) $Cu(OH)_2$, (d) MnCoCu–1:1:1, (e) MnCoCu–3:1:1, (f) MnCoCu–5:1:1, (g) MnCoCu–1:3:1, (h) MnCoCu–1:5:1, (i) MnCoCu–1:7:1, (j) MnCoCu–1:9:1, (k) MnCoCu–1:1:3 and (l) MnCoCu–1:1:5.

Table S1 Calculated elemental composition of as-prepared nanomaterials from EDAX analysis.

S. No.	Sample	Obtained Atom%	Calculated elemental composition
1.	MnO(OH)	Mn (22.19%), O (77.81%)	$Mn_1O_{3.5}$
2.	CoO(OH)	Co (25.65%), O (74.35%)	$Co_1O_{2.9}$
3.	$Cu(OH)_2$	Cu (38.25%), O (61.75%)	$Cu_1O_{1.6}$
4.	MnCoCu–1:1:1	Mn (9.57%), Co (12.14%), Cu (10.81%), O (67.8%)	$Mn_{0.9}Co_{1.1}Cu_1O_{6.2}$
5	MnCoCu–3:1:1	Mn (17.60%), Co (5.32%), Cu (5.33%), O (71.75%)	$Mn_{3.3}Co_1Cu_1O_{13.5}$
6	MnCoCu–5:1:1	Mn (8.50%), Co (2.21%), Cu (2.15%), O (87.14%)	$Mn_5Co_{1.3}Cu_{1.3}O_{51.3}$
7	MnCoCu–1:3:1	Mn (7.13%), Co (21.54%), Cu (7.08%), O (64.25%)	$Mn_1Co_3Cu_1O_9$
8	MnCoCu–1:5:1	Mn (3.74%), Co (23.90%), Cu (4.04%), O (68.33%)	$Mn_{0.8}Co_5Cu_{0.9}O_{14.3}$
9	MnCoCu–1:7:1	Mn (3.48%), Co (24.61%), Cu (3.22%), O (68.69%)	$Mn_1Co_{7.1}Cu_{0.9}O_{19.7}$
10	MnCoCu–1:9:1	Mn (2.90%), Co (26.37%), Cu (2.89%), O (67.84%)	$Mn_1Co_{9.1}Cu_1O_{23.4}$
11	MnCoCu–1:1:3	Mn (8.82%), Co (6.03%), Cu (21.81%), O (63.34%)	$Mn_1Co_{0.7}Cu_{2.5}O_{7.2}$
12	MnCoCu–1:1:5	Mn (4.15%), Co (4.46%), Cu (22.37%), O (69.02%)	$Mn_1Co_{1.1}Cu_{5.4}O_{16.6}$

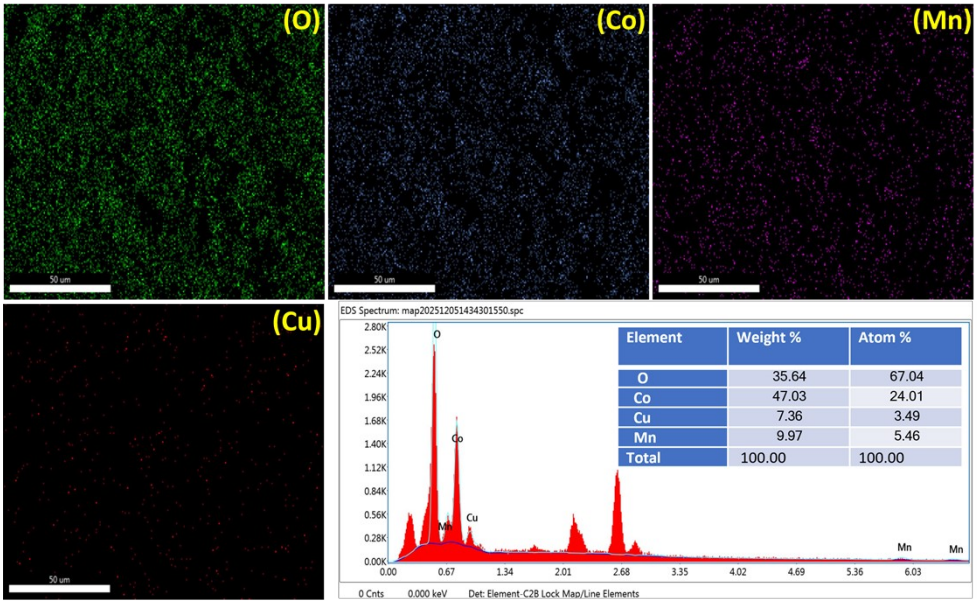

Fig. S5 EDAX elemental mapping images of MnCoCu–1:5:1.

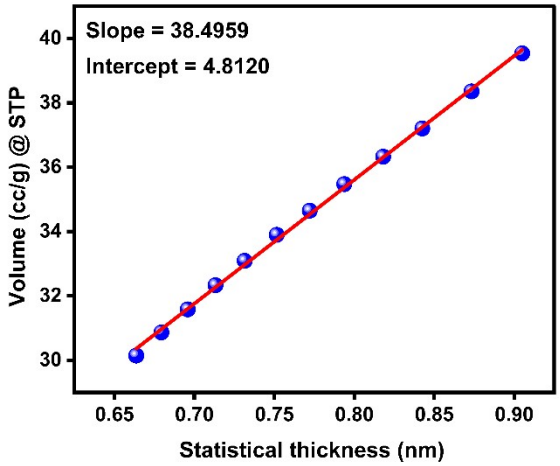

Fig. S6 t-plot (Halsey film-thickness model) for MnCoCu–1:5:1.

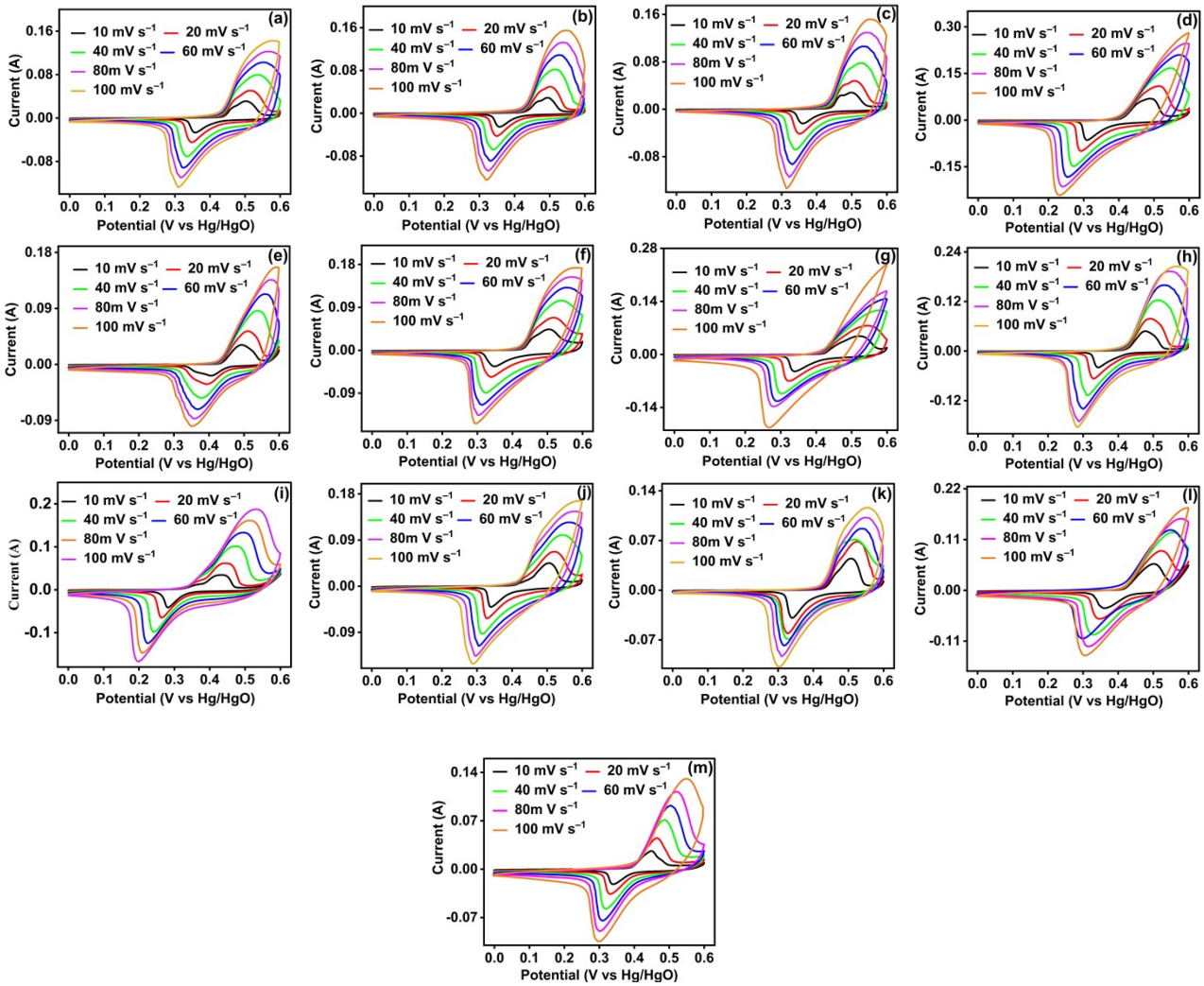

Fig. S7 CV profiles at different scan rates: (a) MnO(OH), (b) CoO(OH), (c) $Cu(OH)_2$, (d) MnCoCu–1:1:1, (e) MnCoCu–3:1:1, (f) MnCoCu–5:1:1, (g) MnCoCu–1:3:1, (h) MnCoCu–1:7:1, (i) MnCoCu–1:9:1, (j) MnCoCu–1:1:3, (k) MnCoCu–1:1:5 (l) MnCo–2:5 and (m) CuCo–2:5.

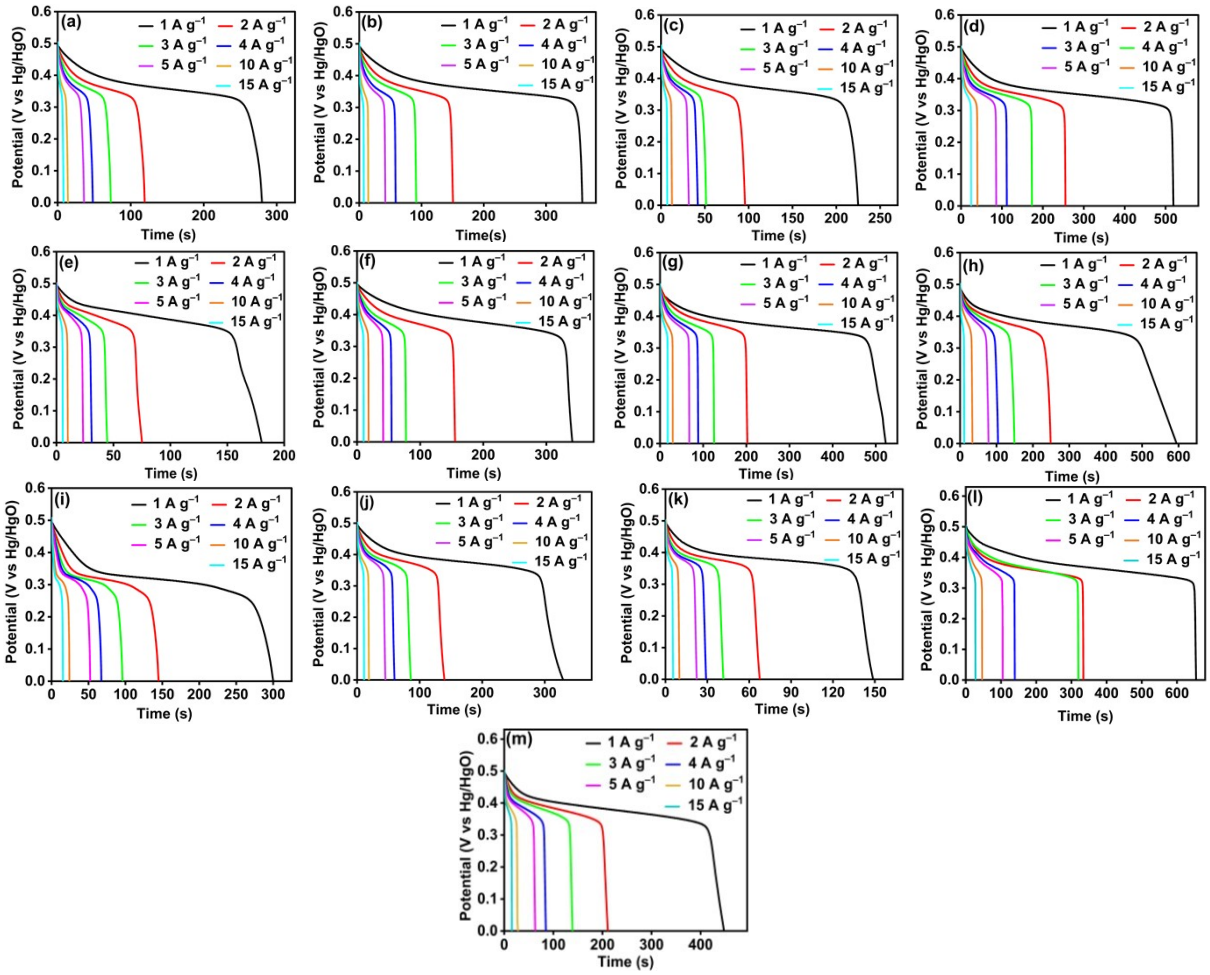

Fig. S8 Discharge curves at different current densities: (a) MnO(OH), (b) CoO(OH), (c) $Cu(OH)_2$, (d) MnCoCu–1:1:1, (e) MnCoCu–3:1:1, (f) MnCoCu–5:1:1, (g) MnCoCu–1:3:1, MnCoCu–1:7:1, (i) MnCoCu–1:9:1, (j) MnCoCu–1:1:3, (k) MnCoCu–1:1:5, (l) MnCo–2:5, and (m) CuCo–2:5.

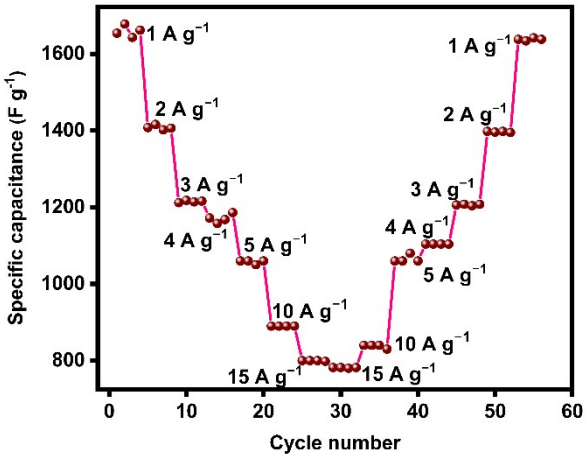

Fig. S9 Rate-capability performance of the MnCoCu–1:5:1.

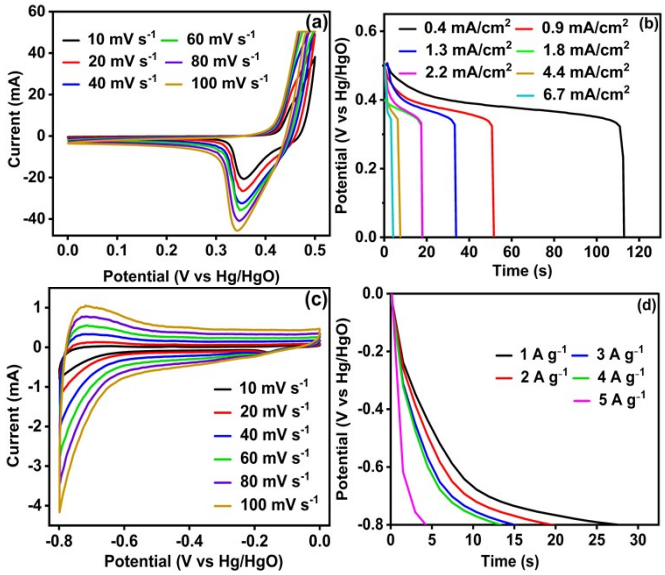

Fig. S10. Cyclic voltammetry profiles at different scan rates (left) and galvanostatic charge–discharge curves at different current densities (right) for (a, b) the bare Ni plate and (c, d) the Ni + C_{AB}/PVDF electrodes.

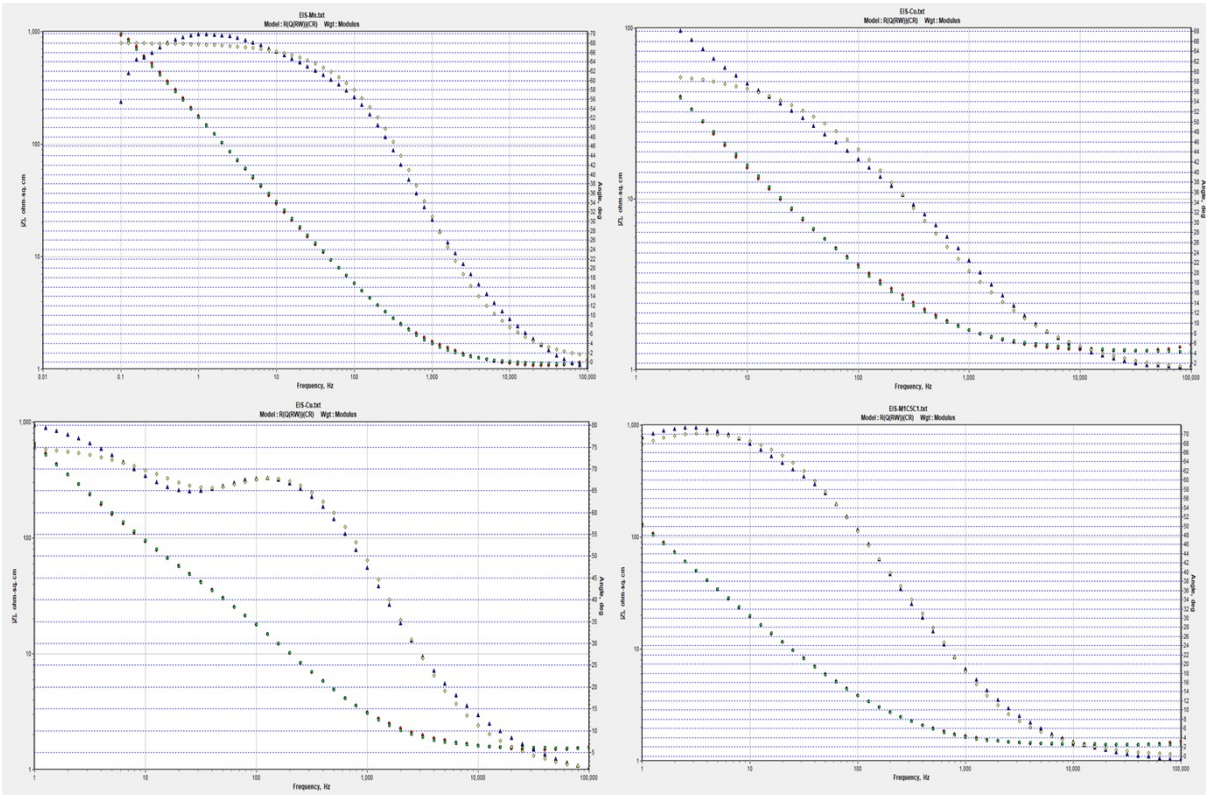

Fig S11. EIS Bode plots of MnO(OH), CoO(OH), $Cu(OH)_2$, and MnCoCu–1:5:1 electrodes.

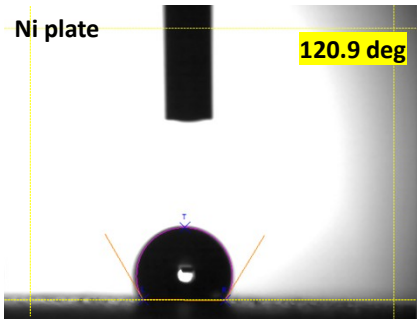

Fig. S12 Contact angle measurement for the bare Ni plate surface using 3M KOH droplet.

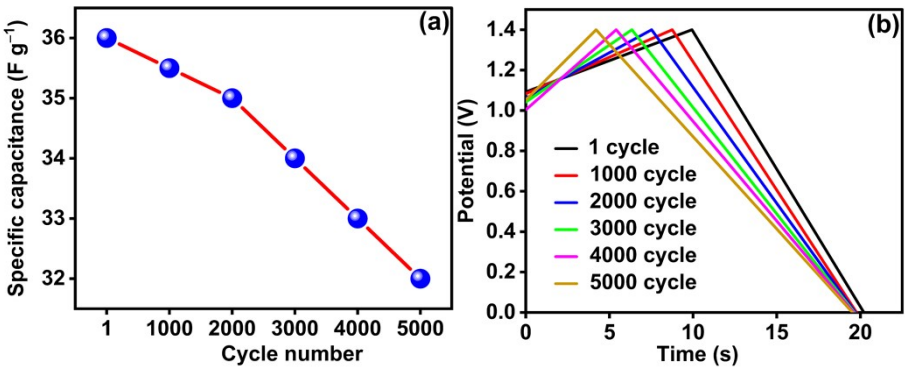

Fig. S13 (a) Specific capacitance versus cycle number and (b) periodic GCD curves of the asymmetric Ni/MnCoCu–1:5:1‖C_{AB}/Ni device measured at a current density of 5 A g^{-1} over 5000 cycles for cyclic stability analysis.

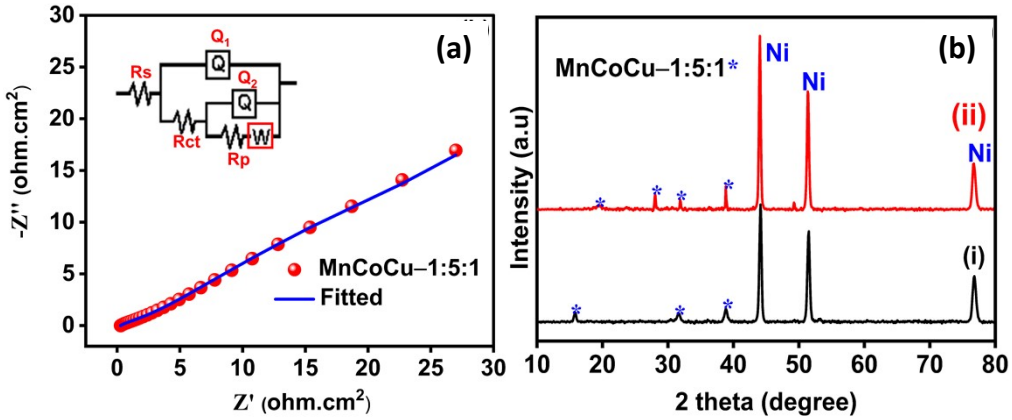

Fig. S14 (a) EIS spectra of the MnCoCu–1:5:1 electrode from the asymmetric device recorded after 5000 GCD cycles in 3 M KOH using a three-electrode configuration; (b) ex-situ XRD of the fabricated MnCoCu–1:5:1 electrode collected before and after 5000 cycles from the asymmetric device.

Table S2 Three-electrode supercapacitor performances for the as-prepared electrode materials at different current densities using 3 M KOH electrolyte.

S. No.	Electrode materials	j (A/g) or *j_A (mA/cm^2)	t_d (s)	η (%)	m_A (mg/cm^2)	ΔV_{IR} (V)	ΔV (V)	C_s (F/g)	Q_s (mAh/g)	C_{areal} (mF/cm^2)	Q_s (C/g)
1	Ni bare	***0.4**	**114**	**99**		**0.02**	**0.48**			**106**	
		*0.9	52	100		0.035	0.465			99	
		*1.3	33	100		0.048	0.452			97	
		*1.8	24	109		0.064	0.436			98	
		*2.2	19	112		0.069	0.431			98	
		*4.4	5	50		0.136	0.364			61	
		*6.7	3	43		0.11	0.39			51	
2	C_{AB}	**1**	**27**	**90**	**0.5333**		**0.8**	**34**	**8**	**18**	**27**
		2	12	100	0.5333		0.8	30	7	16	24
		3	7	78	0.5333		0.8	26	6	14	21
		4	5	100	0.5333		0.8	25	6	13	20
		5	2	100	0.5333		0.8	13	3	7	10
3	MnO(OH)	**1**	**224**	**89**	**0.5333**	**0.06**	**0.44**	**509**	**62**	**272**	**224**
		2	96	92	0.5333	0.01	0.49	392	53	209	192
		3	53	91	0.5333	0.014	0.486	327	44	174	159
		4	42	98	0.5333	0.018	0.482	349	47	186	168
		5	31	97	0.5333	0.022	0.478	324	43	173	155
		10	12	100	0.5333	0.044	0.456	263	33	140	120
		15	6	100	0.5333	0.059	0.441	204	25	109	90
4	CoO(OH)	**1**	**280**	**79**	**0.4889**	**0.07**	**0.43**	**651**	**78**	**318**	**280**
		2	152	87	0.4889	0.011	0.489	622	84	304	304
		3	93	89	0.4889	0.016	0.484	576	78	282	279
		4	58	92	0.4889	0.024	0.476	487	64	238	232
		5	41	93	0.4889	0.031	0.469	437	57	214	205

		10	14	93	0.4889	0.062	0.438	320	39	156	140
		15	8	133	0.4889	0.09	0.41	293	33	143	120
5	$Cu(OH)_2$	**1**	**210**	**84**	**0.5333**	**0.06**	**0.44**	**477**	**58**	**255**	**210**
		2	96	92	0.5333	0.011	0.489	393	53	209	192
		3	52	88	0.5333	0.017	0.483	323	43	172	156
		4	42	98	0.5333	0.02	0.48	350	47	187	168
		5	31	97	0.5333	0.023	0.477	325	43	173	155
		10	12	92	0.5333	0.045	0.455	264	33	141	120
		15	6	86	0.5333	0.065	0.435	207	25	110	90
6	MnCoCu–1:1:1	**1**	**539**	**94**	**0.4444**	**0.003**	**0.497**	**1084**	**150**	**482**	**539**
		2	256	94	0.4444	0.005	0.495	1034	142	460	512
		3	173	95	0.4444	0.007	0.493	1053	144	468	519
		4	112	98	0.4444	0.009	0.491	912	124	406	448
		5	85	98	0.4444	0.011	0.489	869	118	386	425
		10	40	103	0.4444	0.019	0.481	832	111	370	400
		15	25	104	0.4444	0.029	0.471	796	104	354	375
7	MnCoCu–3:1:1	**1**	**182**	**95**	**0.4889**	**0.05**	**0.45**	**404**	**51**	**198**	**182**
		2	75	97	0.4889	0.009	0.491	305	42	149	150
		3	45	100	0.4889	0.013	0.487	277	38	136	135
		4	31	100	0.4889	0.017	0.483	257	34	126	124
		5	23	100	0.4889	0.02	0.48	240	32	117	115
		10	9	100	0.4889	0.035	0.465	194	25	95	90
		15	5	100	0.4889	0.052	0.448	167	21	82	75
8	MnCoCu–5:1:1	**1**	**341**	**113**	**0.5333**	**0.004**	**0.496**	**684**	**95**	**367**	**341**
		2	155	96	0.5333	0.006	0.494	628	86	335	310
		3	77	97	0.5333	0.001	0.499	463	64	247	231

		4	54	98	0.5333	0.013	0.487	444	60	237	216
		5	42	102	0.5333	0.016	0.484	434	58	231	210
		10	18	106	0.5333	0.029	0.471	382	50	204	180
		15	10	100	0.5333	0.043	0.457	328	42	175	150
9	MnCoCu–1:3:1	**1**	**559**	**99**	**0.4444**	**0.003**	**0.497**	**1124**	**155**	**500**	**559**
		2	206	98	0.4444	0.006	0.494	834	114	371	412
		3	126	98	0.4444	0.008	0.492	768	105	341	378
		4	89	100	0.4444	0.01	0.49	727	99	323	356
		5	68	100	0.4444	0.012	0.488	697	94	310	340
		10	29	97	0.4444	0.023	0.477	608	81	270	290
		15	19	112	0.4444	0.033	0.467	610	79	271	285
10	**MnCoCu–1:5:1**	**1**	**839**	**99**	**0.4889**	**0.002**	**0.498**	**1684**	**233**	**824**	**839**
		2	380	99	0.4889	0.002	0.498	1526	211	746	760
		3	235	98	0.4889	0.006	0.494	1427	196	698	705
		4	150	100	0.4889	0.01	0.49	1224	167	599	600
		5	106	98	0.4889	0.012	0.488	1086	147	531	530
		10	42	100	0.4889	0.022	0.478	879	117	430	420
		15	23	105	0.4889	0.033	0.467	739	96	361	345
11	MnCoCu–1:7:1	**1**	**600**	**100**	**0.4444**	**0.002**	**0.498**	**1204**	**167**	**535**	**600**
		2	259	98	0.4444	0.005	0.495	1046	144	465	518
		3	149	96	0.4444	0.008	0.492	909	124	404	447
		4	105	99	0.4444	0.009	0.491	855	117	380	420
		5	79	100	0.4444	0.011	0.489	808	110	359	395
		10	34	103	0.4444	0.019	0.481	707	94	314	340
		15	12	133	0.4444	0.044	0.456	395	50	175	180

12	MnCoCu–1:9:1	**1**	**302**	**88**	**0.4444**	**0.004**	**0.496**	**608**	**84**	**271**	**302**
		2	145	92	0.4444	0.007	0.493	588	81	261	290
		3	96	74	0.4444	0.01	0.49	588	80	261	288
		4	67	96	0.4444	0.012	0.488	549	74	244	268
		5	52	98	0.4444	0.015	0.485	536	72	238	260
		10	24	100	0.4444	0.025	0.475	505	67	225	240
		15	15	100	0.4444	0.037	0.463	486	63	216	225
13	MnCoCu–1:1:3	**1**	**339**	**95**	**0.4444**	**0.004**	**0.496**	**683**	**94**	**304**	**339**
		2	140	97	0.4444	0.008	0.492	569	78	253	280
		3	86	99	0.4444	0.011	0.489	528	72	234	258
		4	60	100	0.4444	0.014	0.486	494	67	219	240
		5	45	100	0.4444	0.017	0.483	466	63	207	225
		10	19	100	0.4444	0.031	0.469	405	53	180	190
		15	11	110	0.4444	0.044	0.456	362	46	161	165
14	MnCoCu–1:1:5	**1**	**148**	**91**	**0.4444**	**0.006**	**0.494**	**299**	**41**	**133**	**148**
		2	68	99	0.4444	0.012	0.488	279	38	124	136
		3	42	100	0.4444	0.017	0.483	261	35	116	126
		4	29	100	0.4444	0.022	0.478	243	32	108	116
		5	23	110	0.4444	0.025	0.475	242	32	108	115
		10	10	111	0.4444	0.044	0.456	219	28	97	100
		15	5	100	0.4444	0.062	0.438	171	21	76	75
15	MnCo–2:5	**1**	**653**	**93**	**0.5333**	**0.006**	**0.494**	**1321**	**181**	**705**	**653**
		2	321	96	0.5333	0.005	0.495	1297	178	692	642
		3	214	96	0.5333	0.007	0.493	1302	178	695	642
		4	140	98	0.5333	0.019	0.481	1164	156	621	560
		5	106	99	0.5333	0.025	0.475	1116	147	595	530
		10	46	100	0.5333	0.041	0.459	1002	128	534	460
		15	29	112	0.5333	0.058	0.442	984	121	525	435

16	CuCo–2:5	**1**	**410**	**85**	**0.5333**	**0.005**	**0.495**	**828**	**114**	**442**	**410**
		2	189	86	0.5333	0.008	0.492	768	105	410	378
		3	119	83	0.5333	0.011	0.489	730	99	389	357
		4	85	100	0.5333	0.012	0.488	697	94	372	340
		5	63	100	0.5333	0.015	0.485	649	88	346	315
		10	26	100	0.5333	0.027	0.473	550	72	293	260
		15	15	100	0.5333	0.039	0.461	488	63	260	225

j (A/g) - Current density (gravimetric); j_A (mA/cm^2) - Areal current density; t_d (s) - Discharge time; η (%) - Coulombic efficiency; m_A (mg/cm^2) - Mass loading; ΔV_{IR} (V) - IR drop; ΔV (V) - Active potential window; C_s (F/g) - Specific capacitance; Q_s (mAh/g) - Specific capacity (gravimetric); C_{areal} (mF/cm^2) - Areal capacitance; Q_s (C/g) - Specific capacity (gravimetric).

Table S3 Two-electrode supercapacitor performances for the as-prepared electrode materials at different current densities using 3 M KOH electrolyte.

S. No.	Electrode materials	j (A/g)	t_d (s)	η (%)	m_A (mg/cm^2)	ΔV_{IR} (V)	ΔV (V)	C_s (F/g)	Q_s (mAh/g)	C_{areal} (mF/cm^2)	Q_s (C/g)	E (Wh/kg)	P (W/kg)
						Symmetric two-electrode studies							
1	Ni/MnCoCu–1:5:1‖MnCoCu–1:5:1/Ni	**0.4**	**117**	**98**	**1.9556**	**0.183**	**1.117**	**42**	**13**	**82**	**47**	**7.3**	**223**
		0.5	77	96	1.9556	0.183	1.117	34	11	67	39	6.0	279
		1	31	89	1.9556	0.337	0.963	32	9	63	31	4.1	482
		2	8	80	1.9556	0.377	0.923	17	4	34	16	2.1	923
						Asymmetric two-electrode studies							
2	Ni/MnCoCu–1:5:1‖C_{AB}/Ni	**0.4**	**782**	**98**	**9.1111**	**0.001**	**1.399**	**224**	**87**	**2037**	**313**	**60.8**	**280**
		0.5	578	99	9.1111	0.001	1.399	207	80	1882	289	56.2	350
		0.6	460	99	9.1111	0.001	1.399	197	77	1797	276	53.6	420
		0.7	334	98	9.1111	0.001	1.399	167	65	1523	234	45.4	490
		0.8	274	99	9.1111	0.001	1.399	157	61	1428	219	42.6	560
		0.9	241	100	9.1111	0.001	1.399	155	60	1413	217	42.1	630
		1	203	99	9.1111	0	1.4	145	56	1321	203	39.5	700
		2	54	98	9.1111	0	1.4	77	30	703	108	21.0	1400
		3	30	100	9.1111	0	1.4	64	25	586	90	17.5	2100
		4	19	100	9.1111	0	1.4	54	21	495	76	14.8	2800

	5	10	100	9.1111	0	1.4	36	14	325	50	9.7	3500

j (A/g) - Current density (gravimetric); t_d (s) - Discharge time; η (%) - Coulombic efficiency; m_A (mg/cm^2) - Mass loading; ΔV_{IR} (V) - IR drop; ΔV (V) - Active potential window; C_s (F/g) - Specific capacitance; Q_s (mAh/g) - Specific capacity (gravimetric); C_{areal} (mF/cm^2) - Areal capacitance; Q_s (C/g) - Specific capacity (gravimetric); E (Wh/kg) – Energy density; P (W/kg) – Power density.

Table S4 Comparison of supercapacitor performance of as-prepared MnCoCu–1:5:1 with reported electrode materials.

S. No.	Electrode materials	Synthetic methodology (material morphology)	Current collector used	Electrolyte	Mass Loading for 3-electrode (mg)	Electrochemical performance				Capacity retention (%) @ number of cycles	Ref.
						3-electrode (C g^{-1} @ ΔV in V)	2-electrode (C g^{-1} @ ΔV in V)	E (Wh kg^{-1}) @ P (W kg^{-1})	Current density (A g^{-1})		
1	MnCo-OH/S-NiCo-OH	Hydrothermal (nanowire)	Ni foam	3 M KOH	2.5	632.52@0.4	219.2@1.6	46.7@800	1	87@ 10,000	11
2	CoMn-HW/rGO	Hydrothermal (nanowire)	Ni foam	3 M KOH	-	290.4@0.55	172.16@1.6	38.3@800	1	89.5@3000	12
3	$NiMoO_4$@$MnCo_2O_4$	Hydrothermal (nanoneedle)	Ni foam	3 M KOH	-	696@0.5	58.53@1.5	90.89@3726	1	96@10000	13
4	$MnCo_2O_{4.5}$@$Co(OH)_2$	Hydrothermal (ribbon)	Ni foam	3 M KOH	1.8	902.52@0.5	249.41@1.6	55.42 @800	1	77.4@4000	14
5	CoMn-LDH/CoMn-S	Electrosynthesis (nanosheets)	Ni foam	3 M KOH	8.4	792.4@0.5	201.3@1.5	82.6@985	1	94 @6000	15
6	CuCoNi-OH	Pyrolysis (leaf-like)	Ni foam	3 M KOH	4.5	821.6@0.5	175@1.6	39.67@400	1	89.8@9000	16
7	Ni–Co–Mn hydroxide	etching process (hierarchical)	Ni foam	3 M KOH	5	757@0.5	219 @1.6	43.1@708	1	83@12000	17
8	NiCoMn hydroxides	Hydrothermal (polyhedral)	Ni foam	3 M KOH	-	817@0.5	185 @1.6	43.9@800	1	72.2@5000	18
9	NiCoMn-OH	Hydrothermal (multi-order hollow)	Ni foam	3 M KOH	1.6-1.8	827@0.4	181@1.6	43.2@0.79	1	100 @10000	19
10	Ni–Co-OH@MnO_2	Hydrothermal (nanoneedle)	Ni foam	3 M KOH	-	1051.3@0.5	126.56@1.5	45@800	1	80@5000	20
11	**MnCoCu-1:5:1 hydroxide/oxyhydroxide**	**Co-precipitation (microspheres/ nanospheres)**	**Ni plate**	**3 M KOH**	**1.1**	**839@0.5 (i.e. 1684 F g^{-1})**	**203@1.4 (asymmetric)**	**39.5@ 700 (asymmetric)**	**1**	**90@5000 (asymmetric)**	**This work**

References

1. S. V. Bhosale and S. V. Bhosale, *Chemical Science*, 2025, **16**, 10159-10227.
2. R. K. Sankaralingam, S. Seshadri, J. Sunarso, A. I. Bhatt and A. Kapoor, *Materials Today: Proceedings*, 2022, **64**, 1649-1654.
3. A. Galarneau, F. Villemot, J. Rodriguez, F. Fajula and B. Coasne, *Langmuir*, 2014, **30**, 13266-13274.
4. P. V. Mane, R. M. Rego, P. L. Yap, D. Losic and M. D. Kurkuri, *Progress in Materials Science*, 2024, **146**, 101314.
5. L. Jing, K. Zhuo, L. Sun, N. Zhang, X. Su, Y. Chen, X. Hu, R. Feng and J. Wang, *Journal of the American Chemical Society*, 2024, **146**, 14369-14385.
6. J. A. Rajesh, J. Y. Park, S. H. Kang and K.-S. Ahn, *Electrochimica Acta*, 2022, **414**, 140203.
7. C. Fang and D. Zhang, *Journal of Materials Chemistry A*, 2020, **8**, 12586-12593.
8. M. Shoeb, F. Mashkoor, J. A. Khan, M. N. Khan, M. A. Gondal and C. Jeong, *Journal of Energy Storage*, 2024, **97**, 112654.
9. S. Suresh, H. C. Prakash, M. S. Kumar and S. K. Batabyal, *Journal of Science: Advanced Materials and Devices*, 2023, **8**, 100639.
10. R. D. Oliveira, C. S. Santos, J. R. Garcia, M. Vidotti, L. F. Marchesi and C. A. Pessoa, *Journal of Electroanalytical Chemistry*, 2020, **878**, 114662.
11. Y.-C. Hsiao, C.-H. Liao, C.-S. Hsu, S. Yougbaré, L.-Y. Lin and Y.-F. Wu, *Journal of Energy Storage*, 2023, **57**, 106171.
12. X. Bai, D. Cao and H. Zhang, *Ceramics International*, 2020, **46**, 19135-19145.
13. Y. Di, J. Xiang, N. Bu, S. Loy, W. Yang, R. Zhao, F. Wu, X. Sun and Z. Wu, *Journal*, 2022, **12**, 1674.
14. M. Xiao, X. Niu, S. Yang, W. Zhang and T. Zhao, *Journal of Solid State Electrochemistry*, 2022, **26**, 1703-1714.
15. M. Moradi, A. Afkhami, T. Madrakian, H. R. Moazami and A. Tirandaz, *Journal of Power Sources*, 2025, **629**, 235993.
16. X. Deng, H. Qin, X. Liu, S. Zhu, J. Li, L. Ma and N. Zhao, *Journal of Alloys and Compounds*, 2022, **918**, 165650.
17. Y. Zhu, C. Huang, C. Li, M. Fan, K. Shu and H. C. Chen, *Journal of Power Sources*, 2019, **412**, 559-567.
18. Y. Chen, J. Yang, H. Yu, J. Zeng, G. Li, B. Chang, C. Wu, X. Guo, G. Chen, L. Zheng and X. Wang, *ACS Applied Energy Materials*, 2022, **5**, 6772-6782.
19. Y. Du, G. Li, M. Chen, X. Yang, L. Ye, X. Liu and L. Zhao, *Chemical Engineering Journal*, 2019, **378**, 122210.
20. F. Wang, Z. Zhao, X. Fu, B. Li, Z. Chen, S. Wang, Q. Huang, Q. Xu and M. Ye, *Journal of Materials Chemistry C*, 2024, **12**, 8004-8013.